AD-A045 216 SOLAR TURBINES INTERNATIONAL SAN DIEGO CA F/G 11/2
STUDY OF EROSION MECHANISMS OF ENGINEERING CERAMICS.(U)
AUG 77 M E GULDEN N00014-73-C-0401
UNCLASSIFIED RDR-1778-8 NL

1 OF 1
AD
A045216

END
DATE FILMED
11-77
DDC

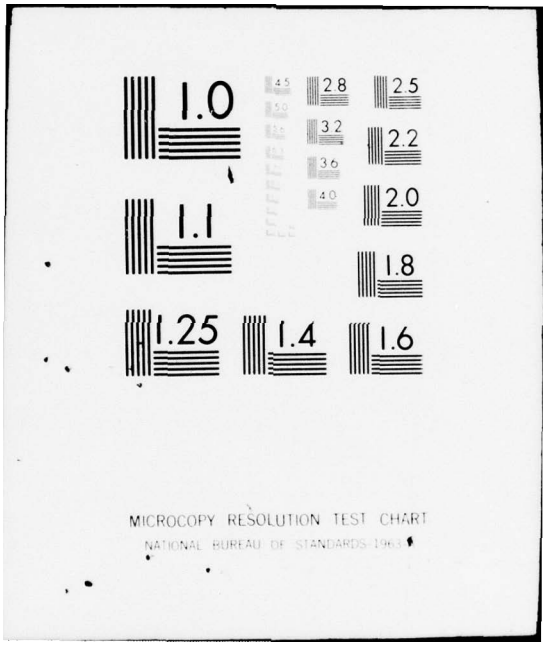
1.0
1.1
1.25
1.4
1.6
1.8
2.0
2.2
2.5
2.8
3.2
3.6
4.0
4.5
5.0
5.6
MICROCOPY RESOLUTION TEST CHART
NATIONAL BUREAU OF STANDARDS-1963-A

August 1977

STUDY OF EROSION MECHANISMS OF ENGINEERING CERAMICS

Sixth Interim Technical Report
April 1 to July 31, 1977

Prepared Under Contract N00014-73-C-0401
NR0-32-542

by
M. E. Gulden

for

OFFICE OF NAVAL RESEARCH
DEPARTMENT OF THE NAVY

Solar Turbines International
an International Harvester Group
San Diego, California

August 1977

STUDY OF EROSION MECHANISMS OF ENGINEERING CERAMICS

Sixth Interim Technical Report
April 1 to July 31, 1977

Prepared Under Contract N00014-73-C-0401
NR0-32-542

by
M. E. Gulden

for

OFFICE OF NAVAL RESEARCH
DEPARTMENT OF THE NAVY

Solar Turbines International
an International Harvester Group
San Diego, California

RDR 1778-8

FOREWORD

This report covers the experimental work performed by Solar from April 1, 1977 to July 31, 1977 on Contract N00014-73-C-0401 sponsored by the Office of Naval Research, Department of the Navy. Relevant observations from previous work on this contract are also included. Dr. A. Diness of the Metallurgy Program is monitoring this contract. The work was performed by Mary Ellen Gulden, Senior Research Engineer, as Principal Investigator under the direction of Dr. Arthur G. Metcalfe, Associate Director of Research. The testing was performed by R. Bradley Domes, Senior Research Technician.

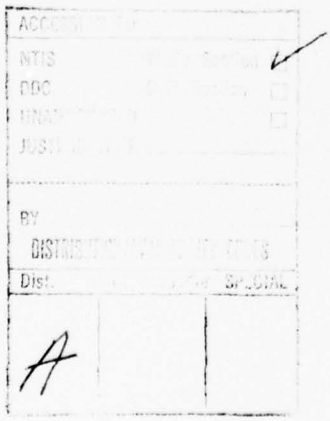

ABSTRACT

Four "engineering" ceramics were subjected to impact (single particle) and erosion (multiple impacts) under conditions which simulate a natural dust environment in the subsonic velocity regime. The target materials are hot pressed Si_3N_4, reaction bonded Si_3N_4, glass bonded Al_2O_3 and hot pressed MgF_2. Tests were performed with 6 narrow size ranges of natural quartz between 10 and 385μ average, and 5 velocities for each particle size. Hot pressed Si_3N_4 was also impacted with SiC under the same particle size velocity conditions.

The results are discussed in terms of current erosion and impact models by considering particle size-velocity dependencies, appearance of the impact damage, and the basic properties and structure of the targets.

Under these erosion conditions, the four target materials exhibited widely different behavior not only in absolute amount of material removed, but also in mechanism of removal. The systems hot pressed Si_3N_4-SiC particles and MgF_2-quartz particles were characterized by plastic impact with associated lateral and radial crack formation, and erosion loss was proportional to particle mass and velocity to the fourth power. Erosion of hot pressed Si_3N_4 impacted with quartz particles was proportional to the first power of particle size and velocity, and loss occurred by minor chipping with no secondary crack formation. Erosion of glass bonded Al_2O_3 and reaction bonded Si_3N_4 did not show a consistent particle size-velocity dependence. The variation is related to the two phase structure of these materials. It was found that strength is not necessarily reduced for erosion conditions which produce appreciable material removal.

TABLE OF CONTENTS

Section		Page
	FOREWORD	ii
	ABSTRACT	iii
1	INTRODUCTION	1
2	EXPERIMENTAL PROCEDURE	1
	2.1 Materials	1
	2.2 Erosion Testing	2
	2.3 Strength Measurements	3
	2.4 Examination of Eroded Surfaces	3
3	EXPERIMENTAL RESULTS AND DISCUSSION	3
	3.1 Erosion Function of Particle Size and Velocity	4
	3.2 Examination of Eroded Surfaces	7
	3.3 Strength of Eroded Specimens	11
	3.4 General Discussion	14
4	CONCLUSIONS	17
	REFERENCES	18
	DISTRIBUTION LIST	

LIST OF FIGURES

Figure		Page
1	Erosion Versus Particle Size and Velocity to the Fourth Power (velocity varied between 40 and 285 m/sec)	5
2	Erosion by Quartz Versus a Measure of Particle Momentum (velocity varied between 40 and 285 m/sec)	6
3	Single Particle Impacts for Systems Which Exhibit Consistent Particle Size-Velocity Functions With Erosion.	8
4	Glass Bonded Al_2O_3 Impacted With 10μ Quartz	11
5	Strength Versus Function of Predicted Radial Crack Formation for Reaction Sintered Si_3N_4 Eroded by Quartz	13
6	Relationship Between Erosion Data and Plastic Impact Model	16

LIST OF TABLES

Table		Page
1	Physical Properties of Target Materials and Particles	2
2	Strength Distribution of Eroded Specimens Relative to Standard Strength	12

1. INTRODUCTION

In recent years, considerable interest has been shown in the use of ceramics for high technology engineering components in such applications as gas turbine engines, bearings, heat exchangers, radomes and infrared transparent windows. All of these applications may involve impingement by solid particles. A knowledge of impact and erosion behavior is necessary before ceramics can be used with confidence in these systems. The materials discussed here, namely NC-132 hot pressed Si_3N_4, NC-350 reaction bonded Si_3N_4, Alsimag 614 glass bonded Al_2O_3 and Irtran 1 MgF_2 are either in current use or considered for potential use in one or more of the above applications.

To date, essentially two types of models have been proposed for impact or erosion of brittle materials (Refs. 1 and 2). The earlier models were based on elastic interaction and predicted that material removal occurs by the intersection of Hertzian ring cracks on the substrate surface. This process has been observed on several materials under static and low velocity impact conditions with relatively large spherical particles (for example, see Ref. 3). More recent analysis has treated static and dynamic plastic indentation which is characterized by plastic deformation of the contact area between the particle and the target, with radial cracks propagating outward from the contact zone, and with subsurface lateral cracks propagating outward on planes nearly parallel to the surface. The former are considered a source of strength degradation and the latter a potential source of material removal. These models are based on single impacts and were developed for isotropic materials under idealized conditions. One objective of this investigation was to assess the validity of these models to predict erosion of engineering ceramics by natural dust environments.

The experimental approach for this investigation has been to perform single impact and erosion (multiple particle impacts) tests in a controlled manner to simulate a service environment in the subsonic velocity regime. This approach advances the understanding of erosion mechanisms of engineering materials as well as providing data of direct value in application of these materials to engineering structures.

2. EXPERIMENTAL PROCEDURE

2.1 MATERIALS

The target materials exhibit a wide range of properties and structure. The properties considered pertinent to erosion response are listed in Table 1. Properties of the particles are also shown.

Angular, high purity quartz particles were used for most of the erosion testing. Quartz was chosen because in previous work on metallic erosion, it had been found to be the principal erosive component in natural dusts, i.e., the amount of erosion was directly proportional to the percentage of quartz in the natural dusts (Ref. 4). Six particle size ranges were used as

Table 1

Physical Properties of Target Materials and Particles

	Elastic Modulus GPa	Fracture Toughness MPa $m^{1/2}$	Hardness[a] GPa	Acoustic Impedance $Kgm^{-2}S^{-1} \times 10^7$	Structure
Hot Pressed Si_3N_4 (NC-132)	320	5	16	3.2	Pseudo single phase - 2μ grain size
Glass Bonded Al_2O_3 (Alsimag 614)	324	3.2	12	4	2-phase - 4% glass, 96% Al_2O_3, 10μ grain size
Reaction Bonded Si_3N_4 (NC-350)	170	2.2	3	2	Multiphase - Si_3N_4 + porosity + Si + SiO_2 (surface)
Hot Pressed MgF_2 (Irtran I)	170	1	6	3.2	Single phase - ∿2μ grain size
Natural Quartz	95	∿0.7	∿6	1.6	
SiC	420	∿3	∿23		

[a] The hardnesses are the quasi-static Vickers hardness in the macro indentation load independent regime.

follows: less than 30, 44-53, 62-74, 105-125, 250-297 and 350-420μm. These size ranges were chosen to be representative of airborne dust and to provide significant particle mass differences of at least 1/2 order of magnitude.

Angular silicon carbide particles of the following size ranges: less than 24, 25-85, 50-165, 203-495, 356-813, and 660-1346μm were supplied by Bendix Abrasives Division. The primary reason for selecting SiC as the second particulate was because of its much higher elastic modulus and hardness compared with quartz. However, the results of the SiC particle tests have direct practical value because it is used as an additive in aircraft carrier antiskid decking.

2.2 EROSION TESTING

Erosion tests were performed with a stationary target impacted by particles accelerated in an air stream. Particles are injected into the stream three meters from the target to provide sufficient distance for acceleration. High pressure, filtered and chemically dried air is used for the particle carrier gas. The carrier air velocity is measured using standard Pitot tube techniques. The air velocity variation across the 0.95 cm diameter nozzle is less than five percent and velocity is varied between 15 and 343 m/sec to achieve the desired particle velocity.

Particle velocity is measured using the rotating double disc technique described in Reference 5. Comparison with calculated velocities based on two phase flow theory is good (Ref. 6). Five velocities for each particle size range were used to establish erosion rates.

All erosion tests were performed at 90 degree impingement angle at ambient temperature. Perpendicular impingement is at or near that for maximum erosion of brittle materials. The number of particles used per test was varied from a few particles (to examine single particle impacts) to as many as 10^8 (to insure initiation of uniform erosion and to avoid incubation effects) over a $0.71 cm^2$ target area. The particles are fed into the gas stream using a precision feeder at a sufficiently low concentration such that particle interactions in the carrier gas stream or on the target surface are negligible. For the longtime-large number of particle tests, the specimens were weighed at specific time intervals to assess any changes in erosion with number of impacts. A detailed description of the erosion test apparatus is given in Reference 6.

2.3 STRENGTH MEASUREMENTS

Strength was determined in three point bending for both forms of Si_3N_4 and the Al_2O_3. Baseline values were obtained on as-received material. To determine a strength loss threshold, strength of eroded specimens was measured over a wide range of test conditions from preweight loss to deeply eroded specimens. Each specimen was visually examined to insure that failure originated in the area subjected to particle bombardment. The eroded areas which are circular of 1 cm diameter were located in the center of the 2.5 or 1.25 cm specimens to insure no extraneous edge effects on strength measurements.

2.4 EXAMINATION OF ERODED SURFACES

The eroded surfaces were examined both optically, and by replica transmission and scanning electron microscopy. The progression of impact or erosion events was monitored by examining the specimens after various number of impacts for several particle size - velocity combinations ranging from single particle impacts to deeply eroded surfaces. The surfaces were also examined in cross section to assess the nature of subsurface damage.

3. EXPERIMENTAL RESULTS AND DISCUSSION

This section is separated into four parts. Initially, the erosion dependence on particle size and velocity will be presented for the 5 target-particle combinations, followed by discussion and examples of the type of impact damage that occurs. Effect of erosion on strength will then be presented, and in the final section a comparison between erosion behavior in terms of impact models and material properties and structure will be made.

3.1 EROSION FUNCTION OF PARTICLE SIZE AND VELOCITY

The customary method of reporting engineering erosion data is by plotting erosion weight loss versus some function of the erosive environment (i.e., particle size, velocity, weight of dust ingested, etc.). Under the same erosion conditions this approach provides a relative ranking of erosion response of the various target materials. Additionally, the phenomenological models proposed for erosion response include dependent functions for particle size and velocity, so that a knowledge of the particle size and velocity dependency of erosion behavior is an important first step to understanding the actual erosion mechanism.

Erosion weight loss as a function of particle mass and velocity was determined for conditions involving millions of particle impacts. This large number of impacts was necessary to insure that uniform erosion is occurring, and that effects from starting surface condition were minimized. In the case of reaction bonded Si_3N_4 (RB Si_3N_4) the as-fired surface layer was removed prior to erosion testing because it was found to erode at a much more rapid rate than the parent material. Weight loss per particle was plotted versus particle radius (log-log plot) and the slopes at constant velocity were measured to determine the particle size exponent. A similar plot of weight loss per particle versus particle velocity yielded the particle velocity exponent at constant particle size.

Two distinct relationships were observed. For the systems, RB Si_3N_4 and MgF_2 impacted with quartz particles and hot pressed Si_3N_4 (HP Si_3N_4) impacted with SiC particles, erosion is proportional to the fourth power of both particle size and velocity. The results are shown in Figure 1 for the three systems. The data is shown as volume loss to give a more meaningful comparison for the different density targets. The relationship between R^4V^4 and erosion is valid over 8 orders of magnitude for MgF_2-Quartz and HP Si_3N_4-SiC, which corresponds to 6 particle size ranges and 5 velocities between 24 and 285 mps for each particle size. The relationship also applies for RB Si_3N_4-Quartz for all particle sizes at higher velocities. These results suggest that a single mechanism is controlling erosion under these test conditions. The data points associated with arrows correspond to weight increases that occurred after low velocity erosion tests on RB Si_3N_4. Since RB Si_3N_4 is an inherently porous ($\sim$25% porosity) material, it is probable that the weight increases correspond to embedding of the quartz particles in the target. This will be discussed later in more detail.

For a given erosion condition with quartz particles, the amount of MgF_2 lost per impact is approximately 1-1/2 orders of magnitude greater than for RB Si_3N_4. HP Si_3N_4 impacted with SiC particles is intermediate between the two.

The system HP Si_3N_4 impacted with quartz particles showed a significantly different erosion dependency on particle size and velocity than the systems previously discussed. Erosion is proportional to particle size to the third power and velocity to the first power which is a measure of particle momentum

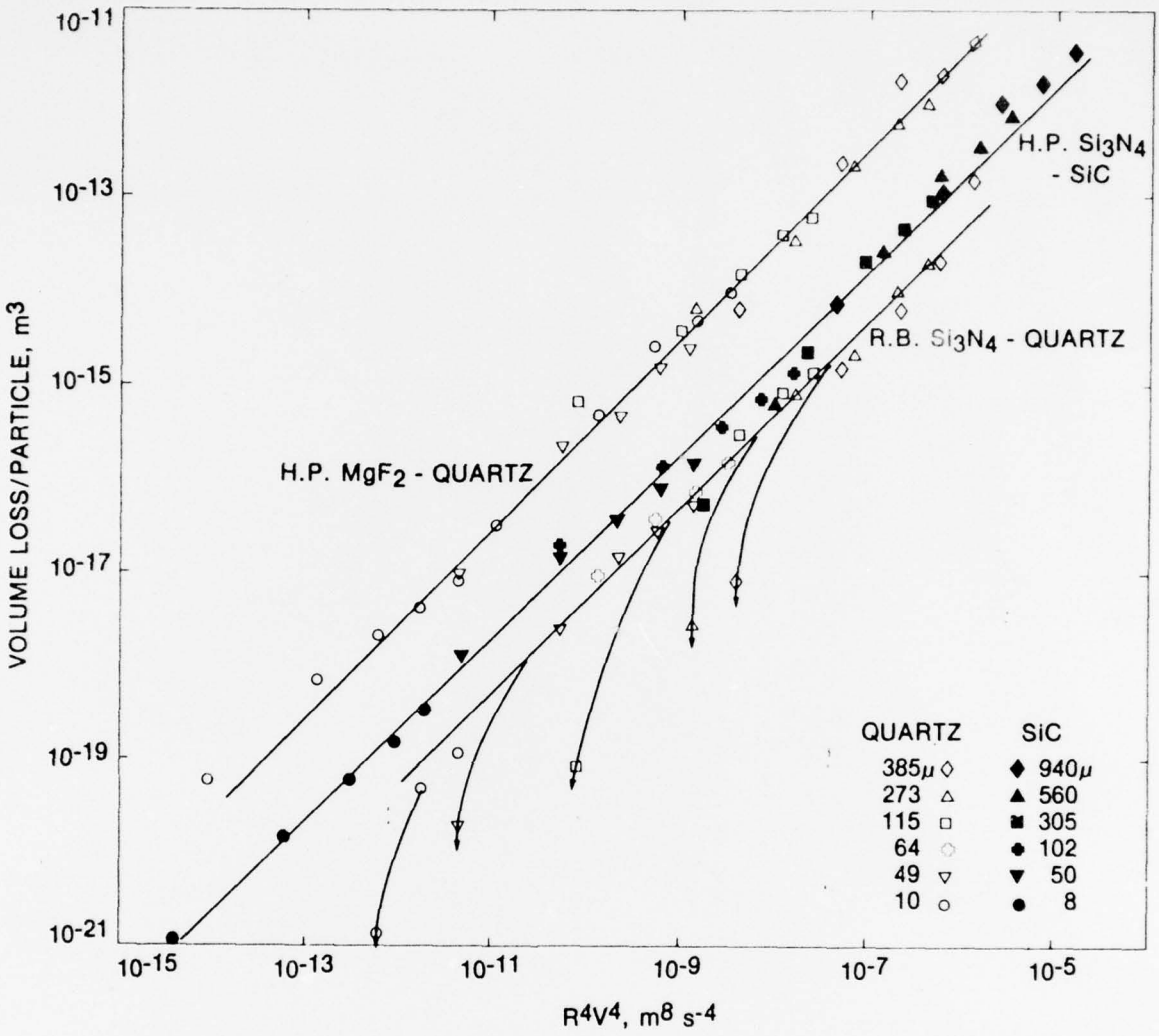

Figure 1. Erosion Versus Particle Size and Velocity to the Fourth Power (velocity varied between 40 and 285 m/sec)

(particle mass times velocity). The results for this system are shown in Figure 2 plotted as volume loss per particle versus a measure of particle momentum. The results are valid over the entire range of particle size - velocity combinations investigated. Deviations from the straight line relationship occur as the volume or weight loss threshold is approached for 115 and 273μ particles. The results for this system indicate that a single mechanism or erosion process is operative within this range of test conditions and that the mechanism of erosion of HP Si_3N_4 by quartz particles is significantly different than the other three target - particle systems which showed a R^4V^4 erosion dependence. For equivalent particle size - velocity tests on HP Si_3N_4, the amount of material lost with SiC impacts was 2 orders of magnitude greater than for quartz impacts (highest velocity tests).

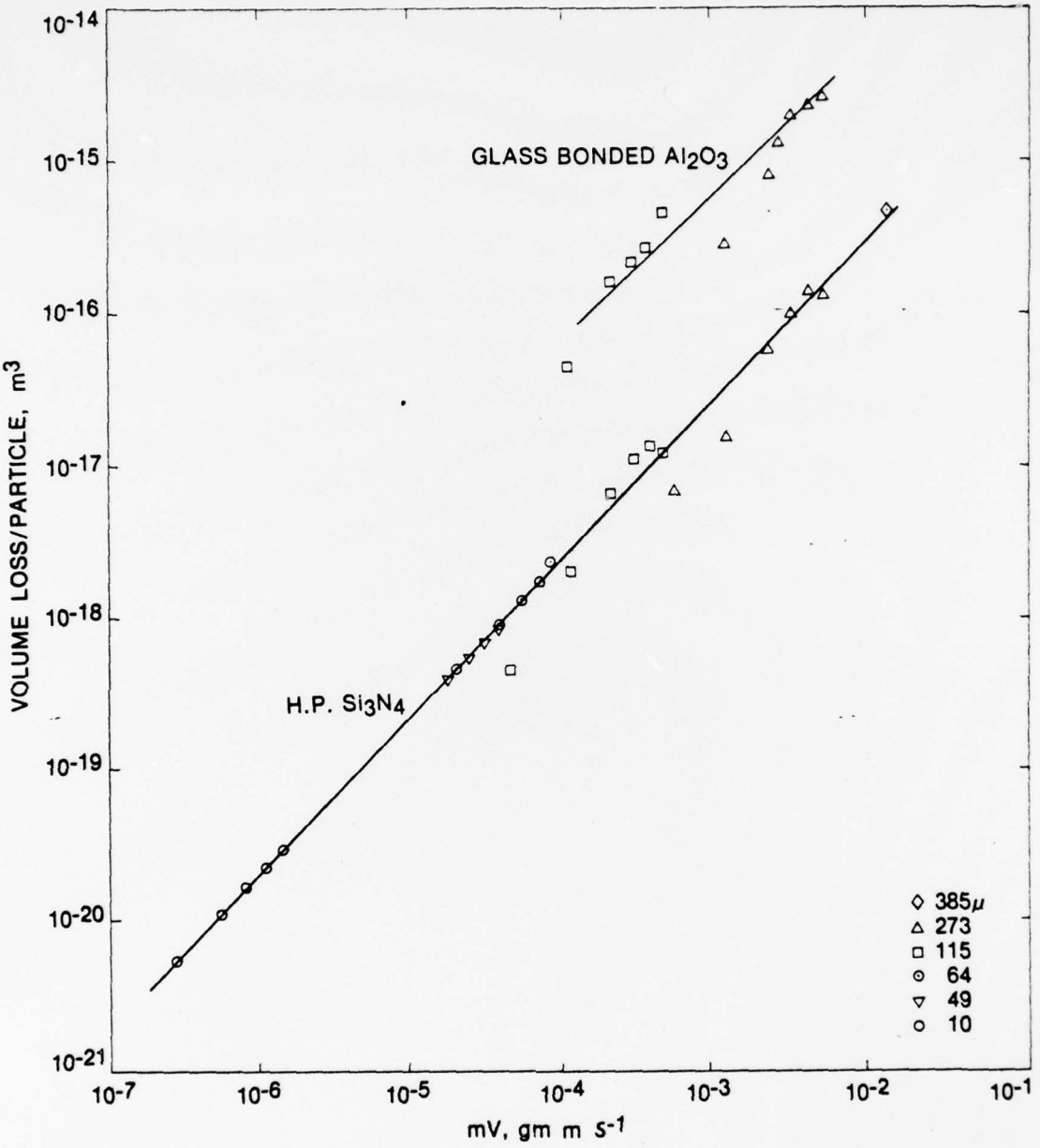

Figure 2. Erosion by Quartz Versus a Measure of Particle Momentum (velocity varied between 40 and 285 m/sec)

Glass bonded Al_2O_3 (GB Al_2O_3) impacted with quartz particles did not exhibit a consistent particle size - velocity dependence. Erosion was proportional to particle radius cubed over the entire range of particle sizes, but the velocity exponent varied between 3 for the smaller particles and one for the larger particles at higher velocities. The test data for erosion with the larger particles is also shown in Figure 2. Apparently, the rate controlling erosion mechanism or process is changing for these test conditions. This change is believed to be related to the 2-phase structure of the target and will be discussed further in the following section.

3.2 EXAMINATION OF ERODED SURFACES

Surfaces were examined for a range of erosion conditions varying between single particle impacts and erosion to a depth of several grain diameters for the various particle size velocity test conditions. Generally, the heavily eroded surfaces were sufficiently damaged that little information was provided concerning erosion mechanisms or processes. However, single particle impacts have provided insight into the process of erosion for these target materials. Figure 3 shows examples of single particle impacts for those target-particle combinations which exhibited a consistent particle-size velocity dependence. The types of impact are typical for each system although magnitude varied with particle size and velocity. The contact areas estimated for purely elastic impact by a spherical particle are given to illustrate variations in damage magnitude. HP Si_3N_4 impacted with SiC particles and MgF_2 impacted with quartz particles (Fig. 3a and 3b) both exhibited plastic impact accompanied by radial and lateral crack formation. The radial cracks extend outward from the particle contact zone and are generally perpendicular to the surface. Lateral cracks also extend from the contact zone but are subsurface and approximately parallel to the surface. This type of impact damage has recently been observed in other systems (Ref. 2). Material removal occurs by loss of a portion or all of the laterally cracked regions. The dark semicircular regions in Figures 3a and 3b correspond to laterally cracked material which has been removed during impact. Also shown in Figure 3a by polarized light reflecting conditions are the lateral cracks which have not resulted in material loss. Since HP Si_3N_4 is opaque, subsurface cracks are not observable by the polarized light technique. For these two systems, the extent of damage or material loss is much larger than the particle contact area.

Figure 3c shows a quartz particle impact on RB Si_3N_4. The impacts in this system are characterized by relatively deep pits with no apparent evidence of secondary cracks intersecting the surface. The approximate calculated contact radius ($\sim$35μ) is of the same order as the pit. The appearance of the pit is one of plastic impact. However, since this material is inherently porous ($\sim$25%), the phenomena could be one of crushing rather than plastic deformation. This porosity might also be expected to arrest crack propagation which would occur in a fully dense material. The type of impact

a. Hot Pressed MgF_2 Impacted With 273μ Quartz

188 m/sec Velocity

Contact Radius ∿27μ

(3 impacts)

b. Hot Pressed Si_3N_4 Impacted With 305μ SiC

176 m/sec Velocity

Contact Radius ∿22μ

Figure 3. Single Particle Impacts for Systems Which Exhibit Consistent Particle Size-Velocity Functions With Erosion (Sheet 1 of 2)

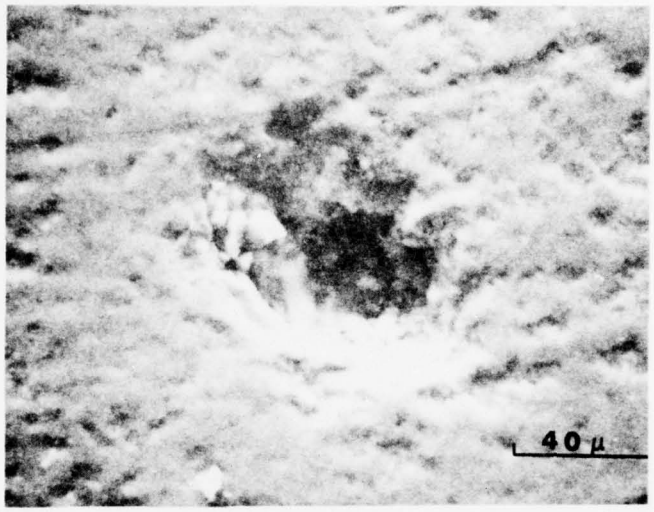

c. Reaction Bonded Si_3N_4 Impacted With 385μ Quartz

174 m/sec

Contact Radius ∿35μ

d. Hot Pressed Si_3N_4 Impacted With 273μ Quartz

188 m/sec Velocity

Contact Radius ∿25μ

Figure 3. Single Particle Impacts for Systems Which Exhibit Consistent Particle Size-Velocity Functions With Erosion (Sheet 2 of 2)

damage shown in Figure 3c is characteristic of the RB Si_3N_4 quartz particle system except for the smallest particles (10μ) where single impacts could not be differentiated from the inherent porosity. Examination in cross section revealed radial cracking beneath the contact area that propagated through the pores.

The type and magnitude of damage produced by quartz particles on HP Si_3N_4 is entirely different from that of the three systems previously discussed. An example is shown in Figure 3d. The chip which has been removed (∿4μ dia) is quite small compared with the approximate calculated contact diameter. For a corner oriented impact with an angular particle the contact area would be smaller and the stresses would be greater.

An estimate of the volume of material removed per impact can be made from the weight loss data on heavily eroded surfaces (data from Figs. 1 and 2). For all of the systems shown in Figure 3, the volume removed per impact for heavily eroded surfaces is within a factor of 2 of that measured from single particle impacts. Considering the statistical nature of the calculations and the test procedure, this shows quite good agreement between single particle impacts and bulk erosion and suggests that secondary cracking and residual erosion damage may not play a significant role in the erosion process under these test conditions.

The discussion to this point in this section has concerned the target-particle systems which exhibited a uniform particle size-velocity relationship over the entire range of test conditions (except low velocity impacts on RB Si_3N_4). The system GB Al_2O_3-Quartz particles did not show a consistent relationship. The structure of this material is characterized by Al_2O_3 grains (∿10μ diameter) surrounded by a glassy intergranular phase. The glass can be as wide as 4μ in the vicinity of grain boundary triple points. It was found that single impact damage for 10μ impacts produced plastic flow in the grain boundary phase and minimal damage to the Al_2O_3 grains. The erosion process occurred by flow and removal of the glass to the extent that entire grains were lost. An example of a surface heavily eroded by 10μ quartz is shown in Figure 4. The depth of erosion corresponds to ∿4 grain diameters. As can be seen, little damage has been sustained by the Al_2O_3 grains. As the particle size was increased, chipping of the Al_2O_3 grains occurred in addition to flow of the glass. This chipping is similar in appearance to that which occurs in the HP Si_3N_4-Quartz system.

Hertzian type cone or ring cracking was not observed for any of these systems under these test conditions.

Examination of the impacted and eroded surfaces has shown that more than one type of impact occurs for this group of target materials under these test conditions. A discussion of the reasons for this variation based on properties and structure of the targets and particles will be given in the General Discussion section.

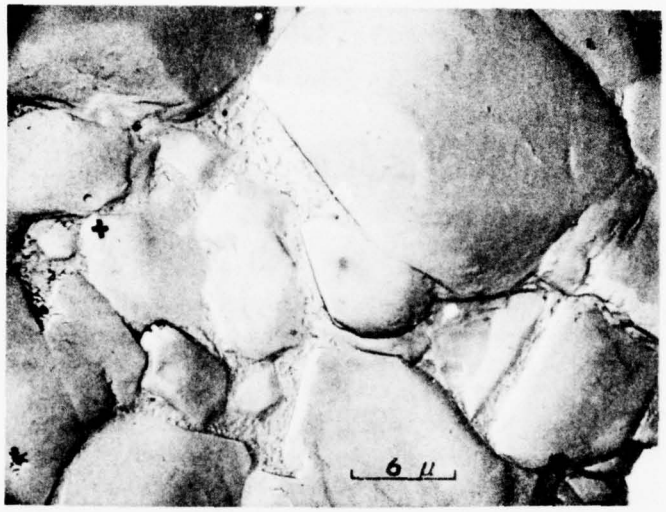

285 m/sec Velocity

Contact Radius ∿2μ

Depth of Erosion ∿50μ

6000 Particle Impacts per Single Particle Contact Area

Figure 4. Glass Bonded Al_2O_3 Impacted With 10μ Quartz

3.3 STRENGTH OF ERODED SPECIMENS

Strength after heavy erosion was determined for HP Si_3N_4, RB Si_3N_4 and GB Al_2O_3 all impacted with quartz particles (same test conditions used to develop Figs. 1 and 2 plus specimens eroded at particle size-velocity conditions below the weight loss thresholds). It was originally expected from Hertzian type considerations that a strength decrease would occur for impact conditions below those needed for actual weight loss, i.e., cracking would occur, but be insufficient to produce material loss. Above the weight loss threshold, strengths were expected to decrease.

The strength results are shown in Table 2. The baseline strengths plus one standard deviation are given for each target material. An estimate of the critical flaw size is also shown. This was calculated from fracture toughness values given in Table 1 using the relationship for three point bend specimens (Ref. 7). The strengths after erosion are shown as a function of the base line strengths by giving the percentages which have strengths greater than +1, within $\pm$1, and less than -1 standard deviation of the noneroded material strength.

HP Si_3N_4 and the GB Al_2O_3 did not exhibit a strength decrease under these test conditions for erosion depths up to 37μ. For HP Si_3N_4 this depth corresponds to 3×10^8 particle impacts or 600 grams of dust on a 0.71 cm^2 area. There was a trend toward strength increase (fracture stress for 50% of the specimens was greater than one standard deviation above the baseline strength) which indicates a "polishing" phenomenon may be occurring. No specimens failed at a stress lower than the one standard deviation band. The erosion depth is approximately three times the estimated critical flaw size

Table 2

Strength Distribution of Eroded Specimens Relative to Standard Strength

	Pre-Erosion Baseline		Post-Erosion Strength Distribution, %				
	$\bar{\sigma}_F \pm 1$ Std. Dev. MPa	% Critical Flaw Size, μ	No. Tests	Max. Erosion Depth, μ	Above +1 Std. Dev.	Within ±1 Std. Dev.	Below -1 Std. Dev.
HP Si_3N_4	798 ± 128	11	25	31	50	50	0
GB Al_2O_3	252 ± 21	43	51	35	41	43	16
RB Si_3N_4	278 ± 10	17	17	360	6	12	82[a]

[a]Minimum Strength = 81 MPa Corresponding to Critical Flaw Size of ∿200μ

which indicates that under these test conditions, the effective flaw size produced by erosion is no larger than pre-existing flaws characteristic of the "standard" machined surface. (Because large numbers of flaws are introduced by erosion or machining, the effective stress concentration will depend on both size and spacing of flaws. In contrast, critical flaw sizes were calculated for isolated flaws.) In confirmation, examination of the eroded surfaces in cross section did not reveal apparent subsurface damage, i.e., the structure under the eroded area was indistinguishable from that below the as-machined surface and subsurface cracking was not apparent.

The trend toward a strength increase is not as conclusive with GB Al_2O_3 as with HP Si_3N_4 since 16% of the specimens failed at stresses below the one standard deviation range. Furthermore, although the maximum depth of erosion (∿35μ) is approximately four grain diameters, this also corresponds to the estimated critical flaw size of the baseline material. However, the results indicate that erosion under these test conditions do not produce flaws greater than those inherent to the as-sintered surface.

RB Si_3N_4 did exhibit a marked strength decrease under these erosion test conditions. Strength decreased rapidly for the first 100μ erosion depth and remained essentially constant at 100 MPa up to the maximum depth tested (350μ). The tests were performed in the as-fired surface condition where the surface oxide layer is ∿100μ deep. The lowest strength (81 MPa) corresponds to an increase in estimated critical flaw size over the baseline material of one order of magnitude (17μ compared with 200μ). The depth of subsurface cracks perpendicular to the surface is also ∿200μ for this erosion condition.

According to the model for plastic impact response, the strength of the target (σ_F) should be dominated by radial crack formation by the following relation:

$$\sigma_F \propto \frac{K_c^{1.4}}{V^{0.5} R^{0.8}}$$ Ref. 2

where K_c is target fracture toughness, V is particle velocity and R is particle radius. A log-log plot of strength versus $(V^{0.5}R^{0.8})^{-1}$ for reaction bonded Si_3N_4 is shown in Figure 5. The data falls roughly into two groups which both have slopes close to one on a log-log basis. The major difference between these two groups is particle size and depth of erosion. The depth of erosion for these particular specimens subjected to 10μ particle bombardment was still within the surface layer which has different material properties and composition than the bulk material. Furthermore, the type of damage and hence flaw type apparently differs from that produced with the larger particles. Subsurface cracking is minor compared with that produced with larger particles, and embedding of the 10μ particles was observed.

Since quartz is the most erosive constituent of natural dusts and the particle size-velocity conditions are typical of airborne dust, these results have direct practical significance, and indicate that a strength decrease does not necessarily occur for erosion conditions which produce appreciable material removal (HP Si_3N_4 and Alsimag 614 glass bonded Al_2O_3). This would be expected to apply as long as the load bearing volume is not reduced significantly.

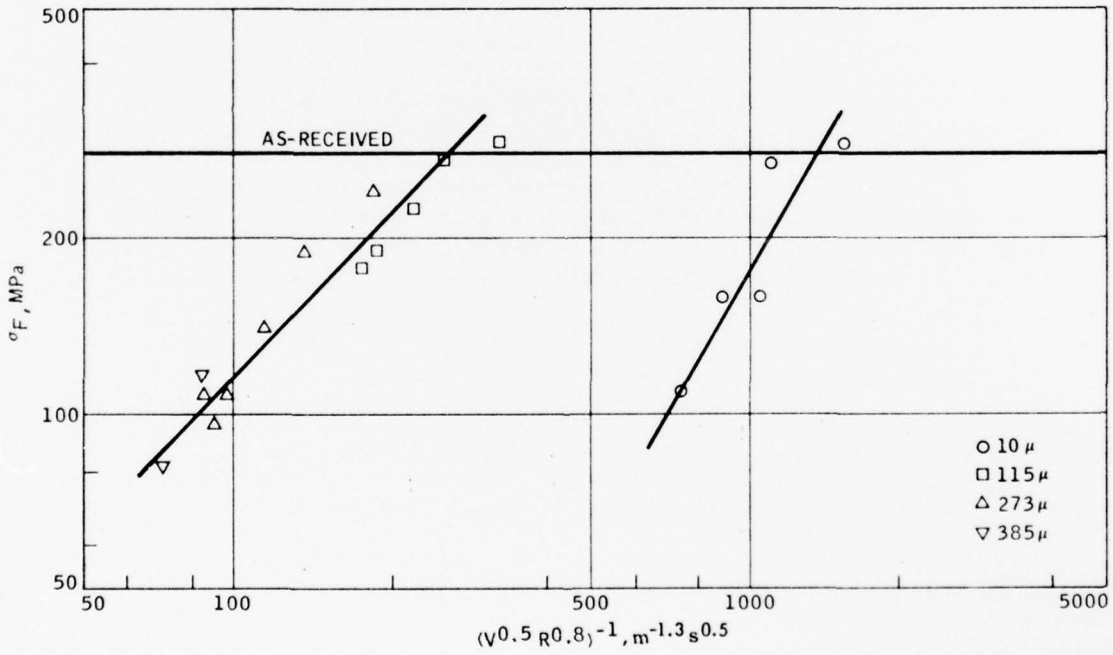

Figure 5. Strength Versus Function of Predicted Radial Crack Formation for Reaction Sintered Si_3N_4 Eroded by Quartz

3.4 GENERAL DISCUSSION

In this section, a comparison will be made between the erosion behavior of the various target materials, and the results will be discussed in terms of impact models and material properties and structure.

Four "engineering" ceramics have been subjected to erosion conditions considered characteristic of a natural dust environment. Under these conditions, the erosion response differs markedly (Figures 1 and 2), and for a given condition, there is approximately one order of magnitude difference in volume loss between each of the targets. There is also considerable variation in material properties and structure between the targets. Table 1 lists the physical properties considered relevant to erosion response. Of the properties listed, fracture toughness is the only property which varied consistently with erosion. The other properties (elastic modulus, hardness and acoustic impedance) would predict either less separation in erosion loss or a different ranking of erosion resistance. Furthermore the particle properties can also have a strong effect on erosion as evidenced by the fact that erosion of HP Si_3N_4 by SiC particles is approximately 2 orders of magnitude greater than with quartz particles for equivalent particle size-velocity test conditions, and the type of impact damage is entirely different.

To date, essentially two types of models have been proposed for solid particle impact or erosion at subsonic velocities. The earlier model was based on Hertzian type purely elastic interaction where material removal occurs by the intersection of ring cracks on the substrate surface. This model was expanded to include Weibull statistics whereby erosion was a function of the distribution and size of flaws under the particle contact area (Ref. 1). This relationship predicted that

$$E \alpha R^4 V^{2.7}$$

(where E is volume removed per particle) for a Weibull modulus greater than 12 and impact with angular particles (Ref. 1). This velocity dependence was not observed for these test conditions, nor was ring cracking.

The second model has treated static, and more recently dynamic, plastic indentation which is characterized by plastic deformation of the contact area between particle and target, radial cracks propagating outward from the contact zone, and lateral cracks that initiate beneath the contact zone and propagate between the radial cracks on planes nearly parallel to the surface. It has been observed for a variety of single phase targets impacted with relatively incompressible projectiles (impact conditions above plastic impact threshold) that the length of radial cracks, and the depth of lateral cracks, for single impacts, followed the relationships predicted by the model (Ref. 2).

If it is assumed that maximum erosion loss per impact is proportional to the volume encompassed by the lateral cracks, then the plastic impact model predicts

$$E \simeq V^{2.5} R^4 \left(\frac{\rho_p}{H K_c^6} \right)^{0.25} f(M)$$

where ρ_p is particle density, H is target hardness, and f(M) is the fraction of the volume encompassed by the lateral cracks that is actually removed and is considered a material dependent variable. Since the experimental erosion data for this type of impact (HP Si_3N_4 impacted with SiC, and MgF_2 impacted with quartz) revealed both a radius and velocity dependence to the fourth power, the term f(M) would have to include a velocity dependence, to obtain conformance with experimental data. This would require that the formation of lateral cracks as well as the volume of laterally cracked material actually removed be velocity dependent.

A log-log plot of $E/V^{2.5}R^4$ versus $\rho_p/H K_c^6$ for the four target materials shows a slope of 0.25 between the 2 target-particle conditions which exhibited typical plastic impact response (Fig. 6). The erosion data in Figure 6 is an average of all of the particle-size velocity test conditions $\pm$ one standard deviation. However, a plot of E/R^4V^4 versus $\rho_p/H K_c^6$ using all of the erosion data (much smaller data band than for $E/R^4V^{2.5}$) also exhibited a slope of 0.25 between HP Si_3N_4-SiC and MgF_2-Quartz.

Erosion for the other target-particle combinations falls below that expected from the plastic impact model although the relative rank is consistent with the model. In the case of HP Si_3N_4 impacted with quartz particles, this is expected since the impact conditions are apparently below the plastic impact fracture threshold (material removal occurs by minor chipping with no apparent secondary crack formation). However, GB Al_2O_3 and RB Si_3N_4 did exhibit plastic deformation.

The model assumes an isotropic material. For the purposes of this investigation, both MgF_2 and HP Si_3N_4 can be assumed to be single phase materials (HP Si_3N_4 contains a minor grain boundary phase, but the 2μ grain size would average this effect over the particle contact area). However, GB Al_2O_3 and RB Si_3N_4 are not single phase materials. RB Si_3N_4 contains ∿25% porosity, and although the impact craters had the appearance of plastic impact, it is possible that crushing is occurring under the contact area. Support for this hypothesis is given by the fact that particles embedded in the surface at low velocities for all particle sizes. Also, the lack of secondary cracking outside of the contact area may be related to the crack blunting ability of the pores. Erosion of GB Al_2O_3 is a two step process which is directly attributable to the two phase nature of the structure.

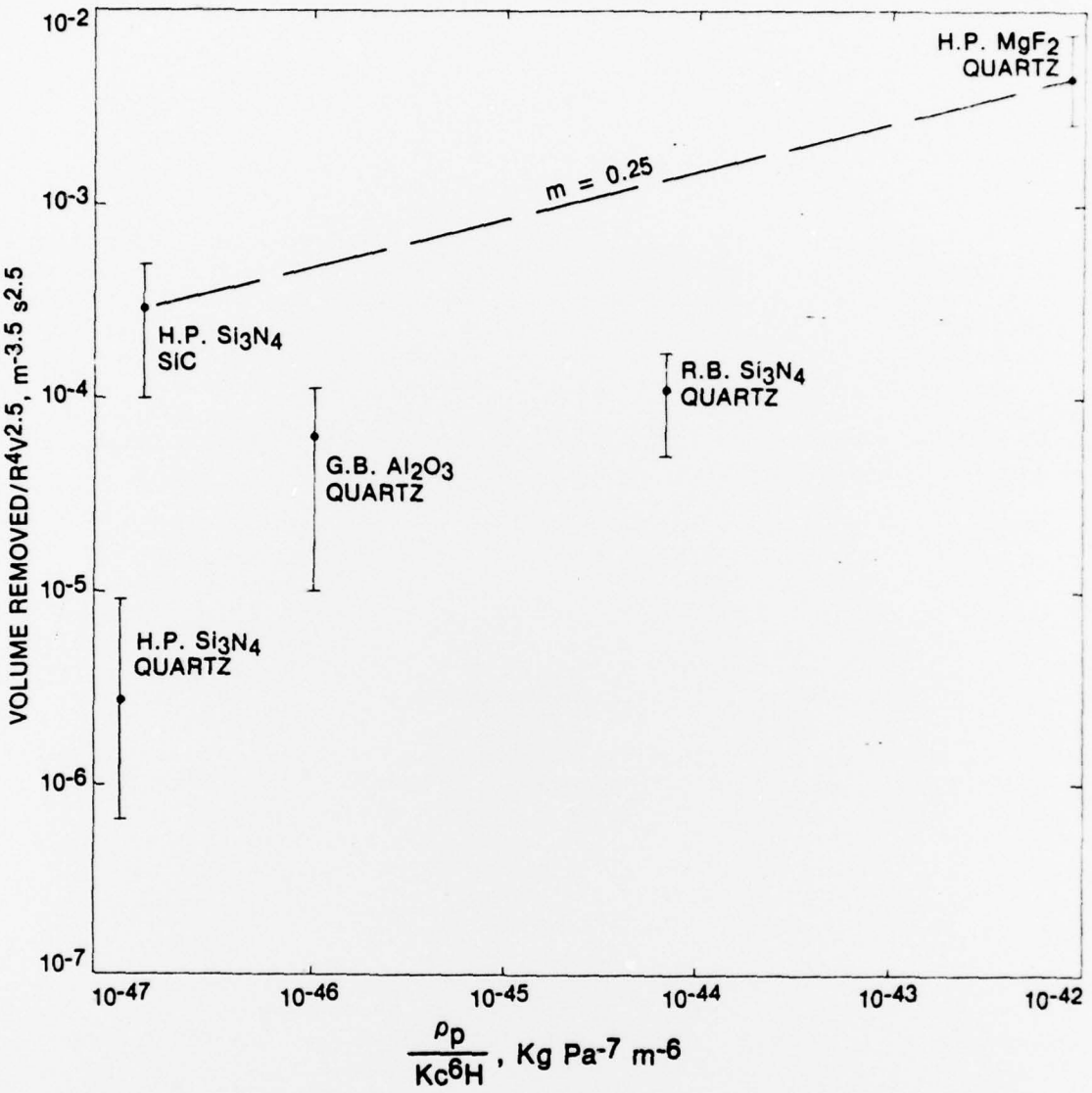

Figure 6. Relationship Between Erosion Data and Plastic Impact Model

The particle composition and properties obviously affect type of erosion response. However, from this investigation only general comments can be made concerning the influence of particle type on erosion of a given target. It appears that for plastic impact response, the particle mechanical properties must closely approach or exceed those of the target. For impact and erosion conditions where the particle properties are appreciably lower than the target, the erosion process is less efficient.

4. CONCLUSIONS

Four ceramic materials with widely different properties and structure were eroded under conditions which simulate a service dust environment i.e., 10-385μ natural quartz particles at subsonic velocities. Additionally, one of the targets (HP Si_3N_4) was impacted with SiC particles over the same particle-size velocity conditions. The following particle size-velocity relationships for erosion were observed:

E	α	R^4V^4	MgF_2-Quartz, RB Si_3N_4-Quartz HP Si_3N_4-SiC
E	α	R^3V	HP Si_3N_4-Quartz
E	α	R^3V^{1-3}	GB Al_2O_3

Single particle damage for the systems HP Si_3N_4 impacted with SiC and MgF_2 impacted with quartz was characterized by plastic impact and radial and lateral cracks propagating from the contact area. The diameter of material removed could be as much as 3 times the contact diameter (corresponds to a portion of lateral crack formation). The diameter of material removed for RB Si_3N_4 was essentially the same as the estimated contact diameter and either plastic deformation or crushing occurred. Erosion of HP Si_3N_4 impacted with quartz occurs by minor chipping which is an order of magnitude less than the estimated contact radius. In the latter two cases, secondary cracking was not observed on the surface. However, RB Si_3N_4 exhibited extensive subsurface radial cracks under the contact area. Erosion on glass bonded Al_2O_3 is a two-step process involving plastic deformation of the glass plus chipping of Al_2O_3 grains.

Based on these results, erosion is a function of particle radius and velocity to the fourth power for a plastic impact response. For a single phase material (HP Si_3N_4, MgF_2) erosion appears to follow the function of fracture toughness and hardness predicted by the model for plastic impact. However, for multiphase materials, structure also influenced erosion response. Below the plastic impact threshold, erosion is a much lesser function of velocity, and elastic ring cracking was not observed. The plastic impact threshold was more a function of target particle type than of particle size and velocity.

Strength measurements after erosion with quartz revealed that strength is not necessarily reduced after conditions which produce significant material removal. (HP Si_3N_4 and GB Al_2O_3 did not show a strength decrease, while RB Si_3N_4 exhibited a major strength decrease.)

It is concluded that more than one mechanism of erosion exists under "natural" dust environments, and that the mechanisms are dependent not only on target physical properties, but also to a large extent on structure.

REFERENCES

1. Oh, H.L., Oh, K.D.L., Vaidyanathan, S. and Finnie, I., *On the Shaping of Brittle Solids by Erosion and Ultrasonic Cutting*,NBS Special Publication 348, 1972, p. 119.

2. Evans, A.G., Gulden, M.E., Eggum, G.E. and Rosenblatt, M., "Impact Damage in Brittle Materials in the Plastic Response Regime," Contract N00014-75-C-0069, Report No. SC5023.9TR, Rockwell International Science Center, Thousand Oaks, CA, 1976.

3. Adler, W.F., "Analysis of Multiple Particle Impacts on Brittle Materials, AFML Tech. Report 74-210, Wright-Patterson Air Force Base, OH, 1974.

4. Smeltzer, C.E., Gulden, M.E., McElmury, S.S. and Compton, W.A., "Mechanisms of Sand and Dust Erosion in Gas Turbine Engines," USAAVLABS Tech. Report 70-36, Fort Eustis, VA, 1970.

5. Ruff, A.W. and Ives, L.K., *Wear*, Vol 35, 1975, p. 195.

6. Gulden, M.E. and Metcalfe, A.G., "Study of Erosion Mechanisms of Engineering Ceramics," Solar Report RDR 1778-4, Solar Turbines International, San Diego, CA, Contract N00014-73-C-0401, 1976.

7. Evans, A.G. in *Fracture Mechanics of Ceramics 1*, R.C. Bradt, D.P.H. Hasselman and F.F. Lange, Ed., Plenum Press, NY, 1974, p. 17.

DISTRIBUTION LIST

BASIC DISTRIBUTION LIST October 1976

Technical and Summary Reports

Organization	No. of Copies
Defense Documentation Center Cameron Station Alexandria, Virginia 22314	(12)
Office of Naval Research Department of the Navy	
Attn: Code 471	(1)
Code 102	(1)
Code 470	(1)
Commanding Officer Office of Naval Research Branch Office 495 Summer Street Boston, Massachusetts 02210	(1)
Commanding Officer Office of Naval Research Branch Office 536 South Clark Street Chicago, Illinois 60605	(1)
Office of Naval Research San Francisco Area Office 760 Market Street, Room 447 San Francisco, California 94102 Attn: Dr. P. A. Miller	(1)
Naval Research Laboratory Washington, D.C. 20390	
Attn: Code 6000	(1)
Code 6100	(1)
Code 6300	(1)
Code 6400	(1)
Code 2627	(1)
Naval Air Development Center Code 302 Warminster, Pennsylvania 18974 Attn: Mr. F. S. Williams	(1)
Naval Air Propulsion Test Center Trenton, New Jersey 08628 Attn: Library	(1)
Naval Construction Batallion Civil Engineering Laboratory Port Hueneme, California 93043 Attn: Materials Division	(1)
Naval Electronics Laboratory Center San Diego, California 92152 Attn: Electron Materials Sciences Division	(1)
Naval Missile Center Materials Consultant Code 3312-1 Point Mugu, California 93041	(1)
Commanding Officer Naval Surface Weapons Center White Oak Laboratory Silver Spring, Maryland 20910 Attn: Library	(1)
David W. Taylor Naval Ship R&D Center Materials Department Annapolis, Maryland 21402	(1)
Naval Undersea Center San Diego, California 92132 Attn: Library	(1)
Naval Underwater System Center Newport, Rhode Island 02840 Attn: Library	(1)
Naval Weapons Center China Lake, California 93555 Attn: Library	(1)
Naval Postgraduate School Monterey, California 93940 Attn: Mechanical Engineering Dept.	(1)
Naval Air Systems Command Washington, D.C. 20360	
Attn: Code 52031	(1)
Code 52032	(1)
Code 320	(1)

Organization	No. of Copies
Naval Sea System Command Washington, D.C. 20362 Attn: Code 035	(1)
Naval Facilities Engineering Command Alexandria, Virginia 22331 Attn: Code 03	(1)
Scientific Advisor Commandant of the Marine Corps Washington, D.C. 20380 Attn: Code AX	(1)
Naval Ship Engineering Center Department of the Navy CTR BG #2 3700 East-West Highway Prince Georges Plaza Hyattsville, Maryland 20782 Attn: Engineering Materials and Services Office, Code 6101	(1)
Army Research Office Box CM, Duke Station Durham, North Carolina 27706 Attn: Metallurgy & Ceramics Div.	(1)
Army Materials and Mechanics Research Center Watertown, Massachusetts 02172 Attn: Res. Programs Office (AMXMR-P)	(1)
Air Force Office of Scientific Research Bldg. 410 Bolling Air Force Base Washington, D.C. 20332 Attn: Chemical Science Directorate Electronics and Solid State Sciences Directorate	(1) (1)
Air Force Materials Lab (LA) Wright-Patterson AFB Dayton, Ohio 45433	(1)
NASA Headquarters Washington, D.C. 20546 Attn: Code RRM	(1)
NASA Lewis Research Center 21000 Brookpark Road Cleveland, Ohio 44135 Attn: Library	(1)
National Bureau of Standards Washington, D.C. 20234 Attn: Metallurgy Division Inorganic Materials Division	(1) (1)
Defense Metals and Ceramics Information Center Battelle Memorial Institute 505 King Avenue Columbus, Ohio 43201	(1)
Director Ordnance Research Laboratory P.O. Box 30 State College, Pennsylvania 16801	(1)
Director Applied Physics Laboratory University of Washington 1013 Northeast Fortieth Street Seattle, Washington 98105	(1)
Metals and Ceramics Division Oak Ridge National Laboratory P.O. Box X Oak Ridge, Tennessee 37380	(1)
Los Alamos Scientific Laboratory P.O. Box 1663 Los Alamos, New Mexico 87544 Attn: Report Librarian	(1)
Argonne National Laboratory Metallurgy Division P.O. Box 229 Lemont, Illinois 60439	(1)

Organization	No. of Copies	Organization	No. of Copies
Brookhaven National Laboratory Technical Information Division Upton, Long Island New York 11973 Attn: Research Library	(1)		
Library Building 50 Room 134 Lawrence Radiation Laboratory Berkeley, California	(1)		

ER
October 1976

SUPPLEMENTARY DISTRIBUTION LIST

Technical and Summary Reports

Dr. W. F. Adler
Effects Technology Inc.
5383 Hollister Avenue
P.O. Box 30400
Santa Barbara, CA 92105

Dr. G. Bansal
Battelle
505 King Avenue
Columbus, OH 43201

Dr. S. A. Bortz
IITRI
10 W. 35th Street
Chicago, IL 60616

Dr. J. D. Buch
Prototype Development Assoc., Inc.
1740 Garry Avenue, Suite 201
Santa Ana, CA 92705

Dr. B. Budiansky
Harvard University
Department of Engineering and
Applied Science
Cambridge, MA 02138

Professor.H. Conrad
University of Kentucky
Materials Department
Lexington, KY 40506

Dr. A. Cooper
Case Western Reserve University
Materials Department
Cleveland, OH 44106

Dr. N. Corney
Ministry of Defence
The Adelphi
John Adam Street
London WC2N 6BB
UNITED KINGDOM

Dr. A. G. Evans
Rockwell International
P.O. Box 1085
1049 Camino Dos Rios
Thousand Oaks, CA 91360

Professor John Field
University of Cambridge
New Cavendish Laboraotry
Cambridge,
UNITED KINGDOM

Dr. I. Finney
University of California
Berkeley, CA 94720

Mr. A. A. Fyall
Royal Aircraft Establishment
Farnborough, Hants
UNITED KINGDOM

Dr. L. M. Gillin
Aeronautical Research Laboratory
P.O. Box 4331
Fisherman's Bend
Melbourne, VIC 3001
AUSTRALIA

Dr. M. E. Gulden
International Harvester Company
Solar Division
2200 Pacific Highway
San Diego, CA 92138

Professor. A. H. Heuer
Case Western Reserve University
University Circle
Cleveland, OH 44106

Dr. R. Hoagland
Battelle
505 King Avenue
Columbus, OH 43201

SUPPLEMENTARY DISTRIBUTION LIST (Cont'd)

Dr. R. Jaffee
Electric Power Research
Institute
Palo Alto, CA

Dr. R. N. Katz
Army Materials & Mechanics
Research Center
Watertown, MA 02171

Dr. H. Kirchner
Ceramic Finishing Company
P.O. Box 498
State College, PA 16801

Dr. B. Koepke
Honeywell, Inc.
Corporate Research Center
500 Washington Avenue, South
Hopkins, MN 55343

Mr. Frank Koubek
Naval Surface Weapons Center
White Oak Laboratory
Silver Spring, MD 20910

Dr. F. F. Lange
Westinghouse Electric Corporation
Research Laboratories
Pittsburgh, PA 15235

Dr. J. Lankford
Southwest Research Institute
8500 Culebra Road
San Antonio, TX 78284

Dr. B. R. Lawn
Physics Department
University New South Wales
Kingston, New South Wales
AUSTRALIA

State University of New York
College of Ceramics at Alfred University
ATTN: Library
Alfrd, NY 14802

Dr. R. E. Loehman
University of Florida
Ceramics Division
Gainesville, FL 32601

Dr. N. MacMillan
Materials Research Laboratory
Pennsylvania State University
College Park, PA 16802

Mr. F. Markarian
Naval Weapons Center
China Lake, CA 93555

Dr. F. A. McClintock
Massachusetts Institute of Technology
Department of Mechanical Engineering
Cambridge, MA 02139

Dr. Perry A. Miles
Raytheon Company
Research Division
28 Seyon Street
Waltham, MA 02154

Dr. D. Mulville
Office of Naval Research
Code 474
800 N. Quincy Street
Arlington, VA 22217

Dr. N. Perrone
Office of Naval Research
Code 474
800 N. Quincy Street
Arlington, VA 22217

Dr. J. R. Rice
Brown University
Division of Engineering
Providence, RI 02912

Dr. R. Rice
Naval Research Laboratory
Code 6360
Washington, DC 20375

SUPPLEMENTARY DISTRIBUTION LIST (Cont"d)

Professor R. Roy
Pen sylvania State University
Materials Research Laboratory
Univeristy Park, PA 16802

Dr. L. Rubin
Aerospace Corporation
P.O. Box 92957
Los Angeles, CA 90009

Dr. G. Schmidt
Air Force Materials Laboratory
Wright-Patterson AFB
Dayton, OH 54533

Dr. D. A. Shockey
Stanford Research Institute
Poulter Laboratory
Menlo Park, CA 94025

Dr. R. A. Tanzilli
General Electric Company
Reentry and Environmental Systems Division
3198 Chestnut Street
Philadelphia, PA 19101

Dr. T. Vasilos
AVCO Corporation
Research and Advanced Development Division
201 Lowell Street
Wilmington, MA 01887

Dr. S. M. Wiederhorn
Inorganic Materials Division
National Bureau of Standards
Washington, DC 20234

Dr. N. Corney
Ministry of Defence
The Adelphi
John Adam Street
London WC2N 6BB
UNITED KINGDOM

Professor John Field
University of Cambridge
New Cavendish Laboratory
Cambridge,
UNITED KINGDOM

Dr. L. M. Gillin
Aeronautical Research Laboratory
P.O. Box 4331
Fisherman's Bend
Melbourne, VIC 3001
AUSTRALIA

Dr. B. R. Lawn
Physics Department
University New South Wales
Kingston, New South Wales
AUSTRALIA

UNCLASSIFIED

SECURITY CLASSIFICATION OF THIS PAGE (When Data Entered)

REPORT DOCUMENTATION PAGE

READ INSTRUCTIONS BEFORE COMPLETING FORM

1 REPORT NUMBER

2 GOVT ACCESSION NO

3 RECIPIENT'S CATALOG NUMBER

4 TITLE (and Subtitle)

Study of Erosion Mechanisms of Engineering Ceramics.

5 TYPE OF REPORT & PERIOD COVERED

Sixth Interim Technical Report.

6 PERFORMING ORG. REPORT NUMBER

RDR-1778-8

7 AUTHOR(s)

Mary Ellen Gulden

8 CONTRACT OR GRANT NUMBER(s)

N00014-73-C-0401

9 PERFORMING ORGANIZATION NAME AND ADDRESS

Solar Turbines International,
an International Harvester Group
PO Box 80966, San Diego, CA 92138

10 PROGRAM ELEMENT, PROJECT, TASK AREA & WORK UNIT NUMBERS

NR032-542

11 CONTROLLING OFFICE NAME AND ADDRESS

Department of the Navy
Office of Naval Research
Arlington, VA 22217

12 REPORT DATE

August 1977

13 NUMBER OF PAGES

19

14 MONITORING AGENCY NAME & ADDRESS (if different from Controlling Office)

12 26p.

15 SECURITY CLASS (of this report)

Unclassified

15a DECLASSIFICATION DOWNGRADING SCHEDULE

16 DISTRIBUTION STATEMENT (of this Report)

Distribution of this document is unlimited.

DISTRIBUTION STATEMENT A
Approved for public release;
Distribution Unlimited

17 DISTRIBUTION STATEMENT (of the abstract entered in Block 20, if different from Report)

18 SUPPLEMENTARY NOTES

19 KEY WORDS (Continue on reverse side if necessary and identify by block number)

Impact	Silicon Nitride	Microscopy
Ceramics	Al_2O_3	
Erosion	MgF_2	
Bend Strength	Mechanical Properties	

20 ABSTRACT (Continue on reverse side if necessary and identify by block number)

Four "engineering" ceramics were subjected to impact (single particle) and erosion (multiple impacts) under conditions which simulate a natural dust environment in the subsonic velocity regime. The target materials are hot pressed Si_3N_4, reaction bonded Si_3N_4, glass bonded Al_2O_3 and hot pressed MgF_2. Tests were performed with 6 narrow size ranges of natural quartz

DD FORM 1 JAN 73 1473 EDITION OF 1 NOV 65 IS OBSOLETE

UNCLASSIFIED

SECURITY CLASSIFICATION OF THIS PAGE (When Data Entered)

326550

between 10 and 385μ average, and 5 velocities for each particle size. Hot pressed Si_3N_4 was also impacted with SiC under the same particle size velocity conditions.

The results are discussed in terms of current erosion and impact models by considering particle size-velocity dependencies, appearance of the impact damage, and the basic properties and structure of the targets.

Under these erosion conditions, the four target materials exhibited widely different behavior not only in absolute amount of material removed, but also in mechanism of removal. The systems hot pressed Si_3N_4-SiC particles and MgF_2-quartz particles were characterized by plastic impact with associated lateral and radial crack formation, and erosion loss was proportional to particle mass and velocity to the fourth power. Erosion of hot pressed Si_3N_4 impacted with quartz particles was proportional to the first power of particle size and velocity, and loss occurred by minor chipping with no secondary crack formation. Erosion of glass bonded Al_2O_3 and reaction bonded Si_3N_4 did not show a consistent particle size-velocity dependence. The variation is related to the two phase structure of these materials. It was found that strength is not necessarily reduced for erosion conditions which produce appreciable material removal.